OPEN ACCESS
JOURNAL OF ADVANCED DIELECTRICS
Vol. 13, No. 3 (2023) 2350009 (8 pages)

DOI: 10.1142/S2010135X23500091

Ferroelectric and piezoelectric properties of lead-free $Li_{0.06}(K_{0.5}Na_{0.5})_{0.94}NbO_3$ thin films

Xinyu Bu, Changhong Yang*, Mengjia Fan, Wenxuan Wang, Xiujuan Lin and Shifeng Huang
Shandong Provincial Key Laboratory of Preparation and Measurement of Building Materials
University of Jinan, Jinan 250022, P. R. China
*mse_yangch@ujn.edu.cn

Received 13 October 2022; Revised 1 February 2023; Accepted 5 March 2023; Published 17 April 2023

Lead-free $(K_{0.5}Na_{0.5})NbO_3$ (KNN) and $Li_{0.06}(K_{0.5}Na_{0.5})_{0.94}NbO_3$ (LKNN) thin films were fabricated by a sol–gel method. The effects of Li substitution on crystal structure, microstructure and electrical properties of KNN film were systematically studied. Li doping can enhance the ferroelectric and piezoelectric properties of KNN film. Compared with pure KNN film, the LKNN film possesses larger remanent polarization (P_r ~ 9.3 μC/cm^2) and saturated polarization (P_s ~ 41.2 μC/cm^2) and lower leakage current density (~ 10^{-5} A/cm^2 at 200 kV/cm). Meanwhile, a typical butterfly shaped piezoelectric response curve is obtained in the LKNN film with a high piezoelectric coefficient (d_{33} ~ 105 pm/V). Excellent fatigue resistance (~ 10^9 switching cycles) and aging resistance (~ 180 days) demonstrate the long-term working stability of LKNN film. These findings indicate that KNN-based lead-free piezoelectric films have a broad application prospect in microelectromechanical systems (MEMS).

Keywords: Lead-free; thin films; $(K_{0.5}Na_{0.5})NbO_3$; sol–gel; piezoelectric property.

1. Introduction

With the rapid development of components toward miniaturization and integration, piezoelectric films have been widely used in microelectromechanical systems (MEMS) such as microsensors, microactuators and energy harvesters.[1–3] Lead zirconate titanate [$Pb(Zr,Ti)O_3$ (PZT)] piezoelectric thin film is regarded as one of the most representative piezoelectric materials and occupies most of the market due to its excellent electrical properties.[4,5] However, considering increasingly serious lead pollution in recent years, lead-free piezoelectric films are urgently needed. Among many lead-free piezoelectric materials, potassium sodium niobate [$(K,Na)NbO_3$ (KNN)]-based materials have been widely studied due to the excellent ferroelectric and piezoelectric properties, and high Curie temperature (T_C = 420°C).[6–9] Several methods have been applied to the fabrication of KNN films, such as RF-sputtering,[10,11] pulsed laser deposition,[12,13] and sol–gel method.[14–17] Among these preparation methods, the sol–gel method is widely used in particular because of its simplicity, low cost and excellent composition uniformity.

Many researchers are committed to improving the piezoelectric and ferroelectric properties of KNN materials through A-site (such as Li) or B-site (such as Sb and Ta) doping.[18,19] However, most studies involve rather complex chemical compositions of Li, Sb and Ta co-doping, making composition inhomogeneity become an inevitable challenge.[20] However, it is reported that doping a small amount of Li ions (< 8 mol%) in KNN is one of the effective ways to improve piezoelectricity.[21–23] In addition, it is also attractive to use only Li due to expensive Ta and toxic Sb. Note that the Li-doped KNN films have a good compositional uniformity because Li, Na and K are all alkali metals. Lin *et al*. reported that $Li_{0.04}(K_{0.5}Na_{0.5})_{0.96}NbO_3$ lead-free piezoelectric thin film with a thickness of 500 nm was annealed at 700°C, and the value of piezoelectric coefficient d_{33} was 48.1 pm/V.[24] Goh *et al*. reported that $0.985K_{0.5}Na_{0.5}NbO_3$–$0.015LiNbO_3$ thin film with a thickness of 1.26 μm was annealed at 700°C, and the value of piezoelectric coefficient d_{33} was 83.1 pm/V.[25] Unfortunately, the d_{33} values of these reported LKNN films are much inferior to that of PZT thin films (~ 300 pm/V),[26] which limits their application in MEMS devices. Many vacancy defects are introduced into the film during the high temperature annealing process due to the volatilization of K and Na ions in KNN film, which directly influences the piezoelectric properties. Therefore, it is still a challenge to fabricate KNN-based films with high piezoelectric coefficient d_{33}.

In this report, the pure KNN film and $Li_{0.06}(K_{0.5}Na_{0.5})_{0.94}NbO_3$ (LKNN) film were prepared by a sol–gel method on Pt/Ti/SiO_2/Si substrates. Excessive 10 mol.% Na and K compensate for alkali volatilization during heat treatment. Both films have a thickness of 800 nm and are annealed at 650°C to appropriately reduce volatilization of alkali ions. The results show that LKNN film has a high piezoelectric coefficient (d_{33} ~ 105 pm/V), which can be attributed to both the preferred orientation and the lattice structure evolution. The LKNN film displays improved ferroelectric properties (P_r ~ 9.3 μC/cm^2) and low leakage current density (~ 10^{-5} A/cm^2 at 200 kV/cm)

*Corresponding author.

without fatigue and aging characteristics. In addition, the leakage mechanism of LKNN film is also revealed, which is dominated by Ohmic mechanism at low electric field and controlled by Fowler–Nordheim (FN) tunneling at high electric field.

2. Experimental Procedure

The lead-free KNN and LKNN films were deposited by a sol–gel method combined with a layer-by-layer annealing process on Pt/Ti/SiO_2/Si substrates. First, sodium acetate [$NaOC_2H_5$] (Sigma-Aldrich, 99%), potassium acetate [KOC_2H_5] (Sigma-Aldrich, 99%), and acetylacetone lithium [$C_5H_7O_2Li$] (Aladdin, 99.9%) were selected as raw chemicals. These materials were dissolved in a solvent of 2-methoxyethanol mixed with acetic acid and refluxed at 70°C for 30 min. Here, 10 mol.% excess sodium (Na) and potassium (K) were added to compensate for the volatilization of alkali ions during the thermal treatment process. This solution was named No. 1. Second, Ethanol niobium [$Nb(OC_2H5)_5$] (Sigma-Aldrich, 99.9%) was added to acetylacetone and acetic acid under the atmosphere of nitrogen, and then, the solution was refluxed at 70°C for 30 min. The solution was called No. 2. With the solution of No. 1 being dropped into No. 2, the final precursor solution with a concentration of 0.3 mol/L was obtained. The solution was aged for at least 24 h to maintain stability.

The prepared precursor solutions were spin-coated onto the Pt/Ti/SiO_2/Si substrates at a speed of 3000 r/min for 30 s. After each layer was deposited, the precursor films were dried on a heating plate at 200°C for 2 min followed by an annealing process at 650°C for 5 min in a rapid thermal processor for complete crystallization. The spin coating and thermal treatment process were repeated several times until the sufficient thickness of films was achieved.

The crystal phase structures of the films were examined by X-ray diffraction (XRD, Bruker D8, Germany) using Cu-Kα radiation. The surface and cross-sectional microstructures of films were observed using an atomic force microscope (AFM, Bruker dimension icon, Germany) and a field-emission scanning electron microscope (FESEM, ZEISS Gemini300, Germany), respectively. The polarization-electric field hysteresis loops and leakage current of the films were evaluated using a ferroelectric tester (aixACCT TF3000, Germany) at room temperature, at the frequency of 10 kHz. An impedance analyzer (Agilent 4294A, USA) was employed to measure the dielectric constant and loss spectra. The piezoelectric properties of the films were characterized by the piezoresponse force microscope (PFM, Bruker dimension icon, Germany).

3. Results and Discussion

Figure 1(a) shows the XRD patterns of KNN and LKNN films deposited on Pt/Ti/SiO_2/Si substrates in the 2θ range of 20°–60°. The diffraction peaks of substrate were also

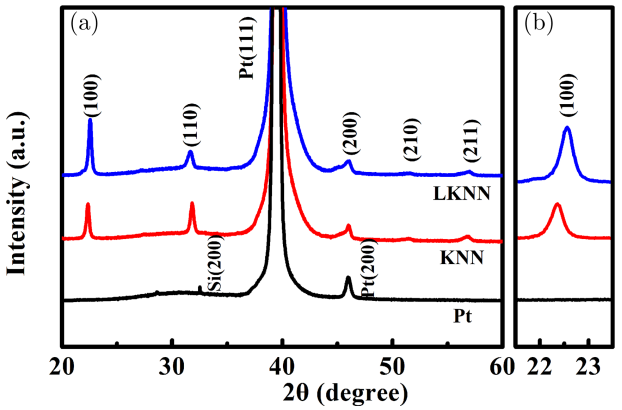

Fig. 1. (a) XRD patterns of KNN and LKNN films; (b) the corresponding magnified patterns of (a) in the vicinity of 2θ = 21.5°–23.5°.

introduced in the figure. Both KNN and LKNN films display an orthorhombic perovskite structure distinctly without secondary phase. It can be proved that the introduction of Li ions has no effect on the structure of the KNN film, and Li ions can enter into the lattice of the KNN perovskite structure. In addition, it should be noted that the (100) peak and the (110) peak show comparable intensity in the XRD pattern of pure KNN. The intensity of (100) peak increases and that of (110) peak decreases when Li is added to the film, suggesting that the LKNN film exhibits a preferred orientation of (100) direction. Compared with the random orientation, the KNN films with preferred orientation of (100) have better piezoelectric properties due to the piezoelectric anisotropy characteristics.[27] Figure 1(b) shows the amplified XRD patterns in the 2θ range of 20.5°–23.5°. Following with the addition of Li ions, the (100) peak slightly shifts to a higher diffraction angle. This is due to the relatively small ionic radius of Li^+ (0.076 nm) compared to Na^+ (0.102 nm) and K^+ (0.138 nm).

Figures 2(a) and 2(b) show the surface images of the region of 2 × 2 μm^2 of the KNN and LKNN films, detected by an AFM. Both films show relatively uniform and dense microstructures, indicating that the films are well crystallized. The average grain sizes of pure KNN film and Li-doped KNN film are 47 nm and 72 nm, respectively. Generally, lithium can be used as a sintering aid and decrease the sintering temperature, which is widely used in the preparation of thin films and bulk materials.[23,24] Thus, the ferroelectric thin film with higher Li content has more sufficient grain growth and larger grain size than the pure KNN thin film under the same annealing condition. Besides, the root mean square roughness (R_{rms}) values of the KNN and LKNN films are 3.6 nm and 4.5 nm, respectively. The film roughness increases with grain growth. Figures 2(c) and 2(d) present the cross-sectional FESEM images of the KNN and LKNN films. The thickness of both films is measured to be approximately 800 nm, and a clear boundary can be observed between the film and the substrate,

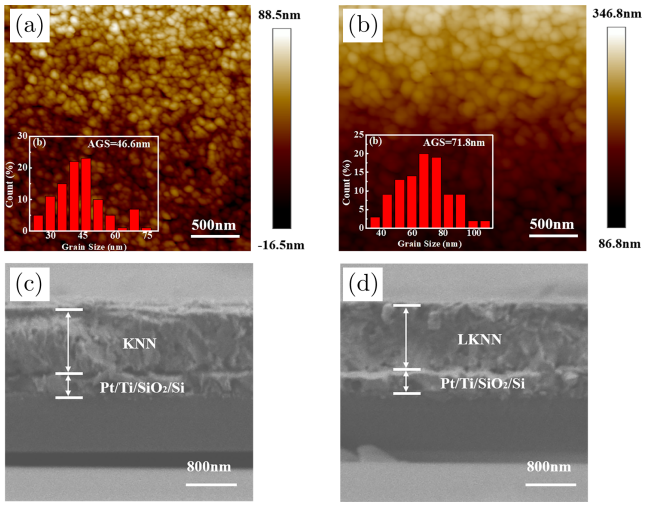

Fig. 2. AFM images of (a) KNN film and (b) LKNN film; cross-sectional field emission scanning electron microscopy (FE-SEM) images of (c) KNN film and (d) LKNN film.

indicating that KNN and LKNN films have been successfully prepared.

Figure 3 presents the frequency-dependent dielectric constant (ε_r) and dielectric loss (tanδ) of KNN and LKNN films tested from 1 kHz to 1 MHz. The values of ε_r for both samples slightly decrease with increasing frequency, which can be explained by the fact that the charges of the interface can follow the change of the alternating current at low frequency, resulting in higher capacitance and dielectric constant.[28] The ε_r values of KNN film and LKNN film are 320 and 360 at 1 kHz, respectively. Compared with pure KNN film, the enhanced ε_r value of Li-doped film is closely related to higher polarization: (i) The substitution of Na and K with Li of smaller diameter supplies larger vibration space in Nb–O octahedron, resulting in enhanced polarization.[28] (ii) In the LKNN film with large grain size, the pinning effect of space charges on domain is weak, which improves the polarization.[29]

In addition, the values of tanδ decrease at first and then increase with the increase of frequency. At low frequency,

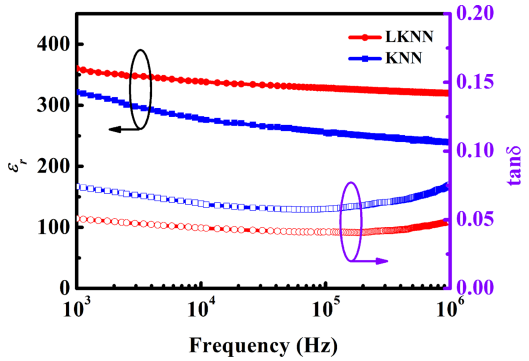

Fig. 3. Frequency dependences of the dielectric constant (ε_r) and dielectric loss (tanδ) for the KNN film and the LKNN film.

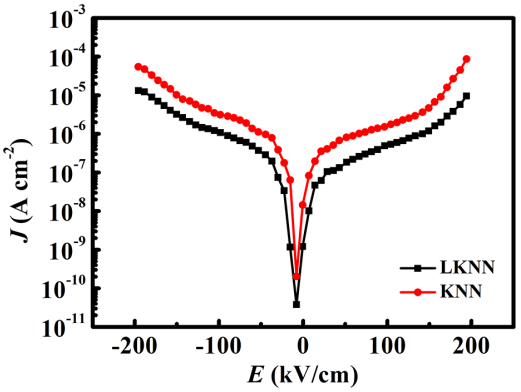

Fig. 4. *J-E* characteristics of KNN and LKNN films on Pt/Ti/SiO_2/Si substrates.

the values of tanδ are mainly affected by leakage current and gradually decrease with the increase of frequency. Therefore, tanδ tends to decrease first at low frequency, while at high frequency, the defect dipole relaxation becomes the main influencing factor. As the frequency continues to increase, the defect dipoles cannot keep up with the frequency change, resulting in the increase of loss.[30,31] The dielectric loss of LKNN film is lower compared to that of KNN film in the whole frequency range, and the value of tanδ is only up to 0.05 at the frequency of 1 kHz, indicating that lithium doping can significantly reduce the dielectric loss.

Figure 4 shows the leakage current density versus electric field (*J-E*) curves measured at room temperature of the undoped and Li-doped KNN films. The leakage current density of both samples increases exponentially with the increase of electric field. Compared with the pure KNN film, the leakage current density of the LKNN film is lower in the whole tested range. For the LKNN thin film, the leakage current density is about 10^{-8} A/cm^2 at the low-electric field of 10 kV/cm, even at the high electric field of 200 kV/cm, the leakage current density is relatively low, in the order of 10^{-5} A/cm^2. It is generally believed that leakage current density is affected by grain boundary content and charged defects. On the one hand, the KNN film has smaller grains and more grain boundaries, which can provide more conduction channels for leakage charges, resulting in greater leakage current density.[32] On the other hand, in the process of heat treatment, a number of cation vacancies and oxygen vacancies are introduced due to the volatilization of K and Na ions in the KNN film, which seriously affects the quality of the film and increases the leakage current of the film. The addition of Li ions compensates the charged defects partly and reduces the leakage current of the film.[33]

Both films represent almost the same asymmetric leakage trend with the electric field, suggesting that the leakage mechanisms are similar for both films. The linear fitting of Li-doped film is carried out under negative and positive biases respectively to explore the leakage mechanism of the film, and the results are shown in Fig. 5(a). According to the fitted

slope values, the log curves of both films can be divided into two regions. In the low-electric field region, the curve fitting slope of both films under positive and negative biases is close to 1.0, which indicates that the conduction mechanism of the film follows the Ohmic mechanism.[34] In the high-electric field region, the fitting slopes of the film suddenly increase.

For clarity, the *J*-*E* curves of LKNN thin film under negative and positive biases have been fitted according to several conduction mechanisms, including space-charge-limited conduction (SCLC), bulk-limited Poole–Frenkel (PF) emission, interface-limited Schottky emission and inter-face-limited FN tunneling, as shown in Fig. 5. These mechanisms can be described by the following equations:[35]

$$J_{\mathrm{SCLC}} = \frac{9\mu\varepsilon_r\varepsilon_0}{8d}E^2, \tag{1}$$

$$J_{\mathrm{PF}} = \mathrm{BE}e^{-\frac{E_I-\sqrt{q^3E/\pi\varepsilon_0K}}{k_BT}}, \tag{2}$$

$$J_S = \mathrm{AT}^2e^{-\frac{\varphi-\sqrt{q^3E/4\pi\varepsilon_0K}}{k_BT}}, \tag{3}$$

$$J_{\mathrm{FN}} = \mathrm{CE}^2e^{-\frac{-D^2-\sqrt{\varphi_i^3}}{E}}, \tag{4}$$

where A, B, C and D are the constants, ε_r is the relative dielectric constant, ε_0 is the permittivity of free space, μ is the charge carrier mobility, d is the film thickness, E is the applied electric field, E_I is the trap ionization energy, q is the electronic charge, K is the optical dielectric permittivity, k_B is the Boltzmann constant, T is the temperature, φ is the Schottky barrier height and φ_i is the potential barrier height.

As shown in Fig. 5(a), the slopes of LKNN thin film in the high electric field region greatly deviate from the ideal value of 2.0, indicating that the SCLC model may not completely illustrate the leakage behavior of the sample in the high-electric field region. Therefore, the other three conduction mechanisms mentioned above will be considered in the following parts.

The K values related to the intrinsic properties have been calculated by the slopes of the fitting lines. The refractive index of pure KNN is known as $n = 2.07$, thus the optical dielectric permittivity is expected to be $K = n^2 = 4.28$.[36] Apparently, the calculated K values for LKNN film shown in Fig. 5(b) are 1.1 and 1.2 under positive and negative biases at high electric field, deviating from the ideal K value, which suggests that the PF emission is not dominant for leakage conduction in LKNN film. Note that K values shown in Fig. 5(c) are 0.4 and 0.5 under positive and negative biases at high electric field, which are much lower than the ideal K value of 4.28, indicating that the Schottky emission is not obvious in LKNN film. Besides, the Ln(J/E^2)-1/E curves of LKNN film are fitted under negative and positive biases, as shown in Fig. 5(d). A superior liner relation between Ln(J/E^2) and 1/E is observed at high electric field, indicating that the leakage current is controlled by FN tunneling.[37,38]

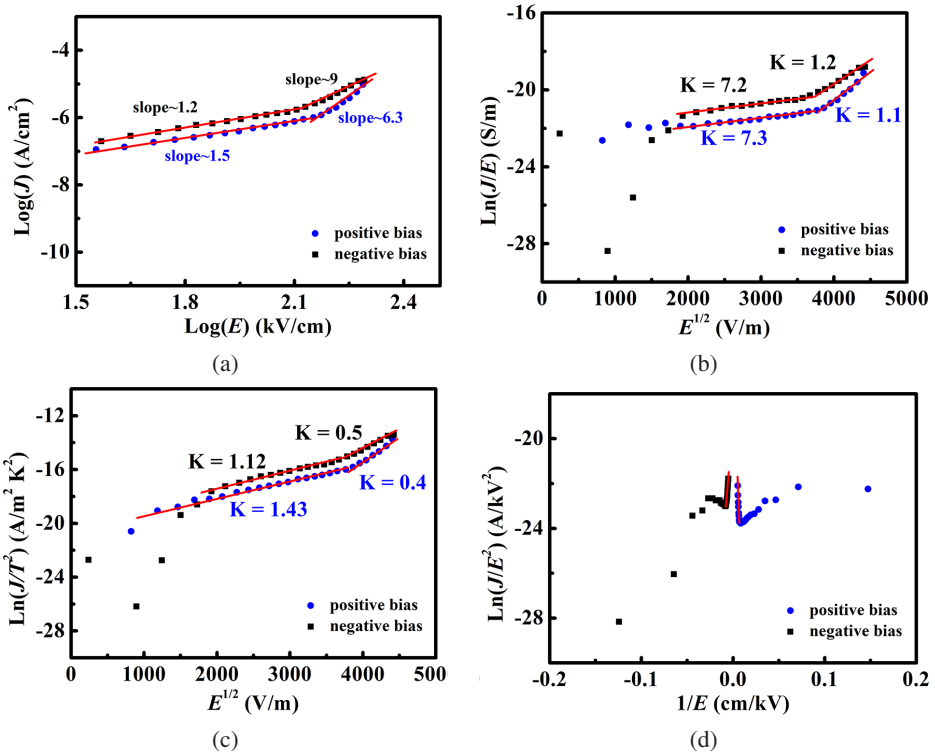

Fig. 5. Plots of leakage current conduction mechanism for LKNN thin film: (a) Log(J)-Log(E), (b) Ln(J/E)-$E^{1/2}$, (c) Ln(J/T^2)-$E^{1/2}$ and (d) Ln(J/E^2)–1/E.

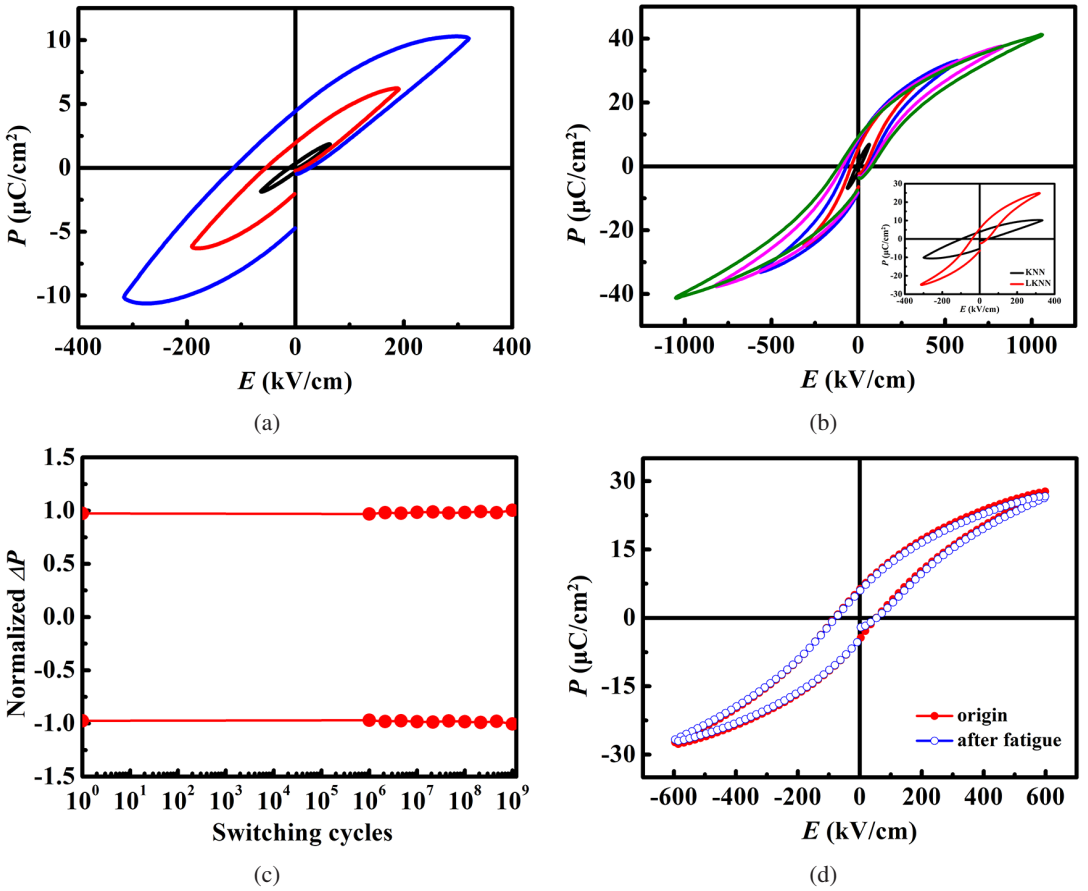

Fig. 6. *P-E* hysteresis loops of (a) KNN film and (b) LKNN film. The inset shows the *P-E* loops for KNN and LKNN films at 320 kV/cm; (c) Normalized pulsed remanent polarization as a function of fatigue cycles; (d) The corresponding *P-E* loops before and after 1×10^9 polarization switching for LKNN film.

Figures 6(a) and 6(b) show the polarization-electric field (*P-E*) hysteresis loops of the pure KNN film and the LKNN film as a function of applied electric field at 10 kHz. The *P-E* loops of both films exhibit increased polarization with the increase of electric field due to enhanced domain flipping. Pure KNN film only represents the *P-E* loop at low electric field and shows a small remanent polarization of 4.5 μC/cm^2, and a coercive field (E_c) of 25.9 kV/cm, under an electric field of 320 kV/cm. Under the same electric field, LKNN film exhibits higher remanent polarization (P_r ~ 5.6 μC/cm^2) and smaller coercive field (E_c ~ 23.7 kV/cm) due to the addition of lithium to compensate for the charged defects, as shown in the inset of Fig. 6(b). The full *P-E* loop and low electric field resistance of pure KNN film can be attributed to the increase of leakage current. However, the LKNN film can be subjected to higher electric field, which exhibits well-defined ferroelectric responses and a thin *P-E* loop. The LKNN film achieves a high P_r of 9.3 μC/cm^2, and a P_s of 41.2 μC/cm^2 even at a high applied electric field of 1050 kV/cm.

Fatigue characteristics are an important means to evaluate the working durability of ferroelectric thin film capacitors. Figure 6(c) shows the normalized pulsed remanent polarization (ΔP) as a function of switching cycles for the LKNN film measured at an electric field of 600 kV/cm. After 10^9 switching cycles, the ΔP of the LKNN film maintains stable. Figure 6(d) shows the *P-E* hysteresis loops of the LKNN film in fatigue test. The values of P_r, P_s and E_C show slight changes with a small variation range (less than 6.3%, 4.1% and 5.9%, respectively) after 10^9 fatigue cycles, representing fairly satisfactory fatigue characteristics.

To investigate the aging characteristics of LKNN film, the *P-E* loops of the same sample after different aging days at room temperature were tested at an electric field of 500 kV/cm, as shown in Fig. 7(a). Noticeably, although the LKNN film has been placed for a long period (~180 days), the shape of its *P-E* loop has barely changed. Specific parameter values are shown in Fig. 7(b). The values of P_r, P_s and E_c for the LKNN sample decrease slightly. This result is owing to the enhanced pinning effect of defect dipoles ($[2V'_A - V^{\bullet\bullet}_O]$, A could be Na, K, Li) on part of domains with increasing aging time.[39,40] The variation values of P_r, P_s and E_c are only 6.6%, 7.6% and 2.7%, respectively, showing the excellent stability of the placement time.

To characterize the piezoelectric properties of pure KNN and LKNN films on Pt/Ti/SiO_2/Si substrates, switched spectrum PFM technique was used to monitor the phase and

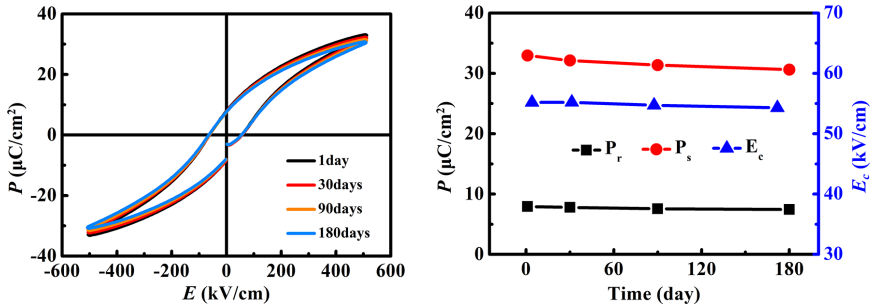

(a) (b)

Fig. 7. (a) *P-E* loops evolution process of the LKNN film after 1 day, 30 days, 90 days and 180 days; (b) P_s, P_r and E_c values for the LKNN film as a function of time.

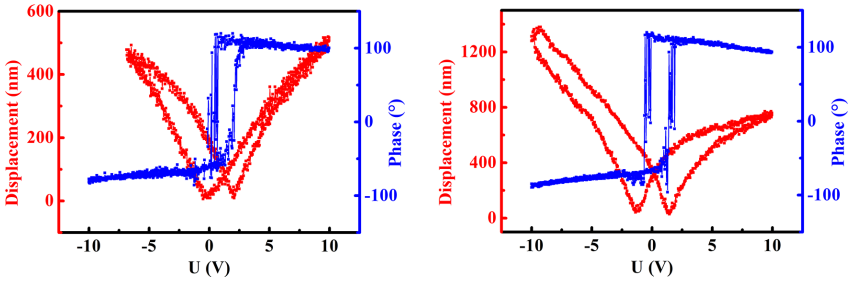

(a) (b)

Fig. 8. Displacement–voltage loops and phase–voltage loops of (a) KNN film and (b) LKNN film.

Table 1. Electrical properties of $(K_{0.5}Na_{0.5})NbO_3$ and $(K_{0.5}Na_{0.5})NbO_3$-based films.

Composition	Substrate	Preparation method	Annealing temperature (°C)	Thickness (nm)	P_r (μC/cm^2)	ε_r	d_{33}^* (pm/V)	Ref.
$K_{0.5}Na_{0.5}NbO_3$	Pt/Ti/SiO_2/Si	Chemical solution deposition (CSD)	650	600	7		46	44
$K_{0.5}Na_{0.5}(Nb_{0.7}Ta_{0.3})O_3$	Pt/Ti/SiO_2/Si	CSD	700	500	10.5		61	49
$K_{0.5}Na_{0.5}(Mn_{0.005}Nb_{0.995})O_3$	Pt/Ti/SiO_2/Si/SiO_2/ banding layer	CSD		1000	10		90	45
$K_{0.44}Na_{0.52}Li_{0.04}Nb_{0.84}Ta_{0.1}Sb_{0.06}O_3$	$SrRuO_3$/$SrTiO_3$	Pulsed laser deposition (PLD)	750	500	7.5	330	53	50
$(K_{0.44}Na_{0.52}Li_{0.04}Nb_{0.86}Ta_{0.1}Sb_{0.04})O_3$	Pt/Ti/SiO_2/Si	Radio Frequency (RF)	750	350	8.6		21	46
$K_{0.4425}Na_{0.52}Li_{0.0375}Nb_{0.8825}Sb_{0.08}Ta_{0.0375}O_3$	Pt/Ti/SiO_2/Si	Sol–gel	750	300	9.5	341		51
$Li_{0.04}(K_{0.5}Na_{0.5})_{0.96}NbO_3$	Pt/Ti/SiO_2/Si	Sol–gel	700	500	14.3		48.1	24
$0.95K_{0.5}Na_{0.5}NbO_3$-$0.05LiNbO_3$	Pt/Ti/SiO_2/Si	Sol–gel	700	1260		259	83.1	25
This work	Pt/Ti/SiO_2/Si	Sol–gel	650	800	9.3	360	105	

displacement hysteresis loops by applying a bipolar driving voltage of −10 V to +10 V between the top and bottom electrodes. Signals were obtained from OFF sates to eliminate the interference of electrostatic force.[41] Both samples exhibit typical butterfly displacement-voltage loops with 180° domain switching under applied voltage, which reflects the contribution of domain wall motion,[42] as shown in Fig. 8. It is observed that both samples show some degree of displacement under zero electric field, which may be due to the fact that the domains do not normally switch to the original positions under zero field. According to the converse piezoelectric effect, the value of d_{33} is calculated by the following equation:[43]

$$d_{33} = (D_i - D_0)/(U_i - U_0), \quad (5)$$

where U_i and D_i are the voltage and displacement at any single point, U_0 and D_0 are the intersections of the butterfly curve.

The piezoelectric coefficient d_{33} of pure-KNN film is about 48 pm/V, which is equal to that of sol–gel-derived KNN film reported by Nakashima *et al*.[44] The LKNN film has a significantly increased d_{33} value of 105 pm/V, which is higher than that of 0.5 mol% Mn-doped KNN film (d_{33} ~ 90 pm/V)[45] and $(K_{0.44}Na_{0.52}Li_{0.04})(Nb_{0.86}Ta_{0.10}Sb_{0.04})O_3$ film (d_{33} ~ 21 pm/V).[46] Compared with the pure KNN film, the enhanced piezoelectric properties can probably be attributed to the following aspects: (i) The increased (100) orientation of the film caused by lithium substitution.[27] (ii) The doping of the smaller Li ions caused lattice distortion, which promotes the domain wall movement.[47,48]

Table 1 summarizes the preparation processes and electrical properties of different KNN and KNN-based films in detail.

It can be seen that the annealing temperature of KNN-based films is usually high (above 700°C), which leads to the volatilization of a large number of K and Na ions in KNN-based films and directly affects the piezoelectric properties. By proper lithium doping and optimized annealing temperature, our LKNN film improves piezoelectric coefficient d_{33} while maintaining ferroelectric and dielectric properties comparable to those of KNN-based films reported by others.

4. Conclusion

In summary, the pure KNN and Li-doped KNN films with perovskite structure were successfully deposited on Pt/Ti/SiO_2/Si substrates by a sol–gel method. The surface morphology and leakage current characteristics of the KNN film can be improved by introducing a small amount of Li ions. *P-E* tests show that LKNN film represents a well-saturated *P-E* hysteresis loop. Compared with pure KNN film, LKNN film possesses superior ferroelectric properties with a high P_r of 9.3 μC/cm^2, and a P_s of 41.2 μC/cm^2. Meanwhile, excellent aging resistance and ferroelectric fatigue resistance up to 10^9 cycles can be achieved in the LKNN film, showing the long-term stability. In addition, the piezoelectric properties of KNN film are significantly improved by Li substitution and the d_{33} value of the LKNN film is 105 pm/V. The results show that LKNN film has potential for applications in the piezoelectric MEMS devices.

Acknowledgments

This work was supported by the National Natural Science Foundation of China (Grant Nos. 51972144 and U1806221), the Taishan Scholars Program, the Case-by-Case Project for Top Outstanding Talents of Jinan, the Shandong Provincial Natural Science Foundation (Grant No. ZR2020KA003), the Primary Research & Development Plan of Shandong Province (Grant No. 2019JZZY010313), the Project of "20 Items of University" of Jinan (Grant Nos. T202009 and T201907), and the Introduction Program of Senior Foreign Experts (G2021024003L).

References

[1]K. A. Cook-Chennault, N. Thambi and A. M, Sastry, Powering MEMS portable devices-a review of non-regenerative and regenerative power supply systems with special emphasis on piezoelectric energy harvesting systems, *Smart. Mater. Struct.* **17**, 043001 (2008).

[2]S. Tadigadapa and K. Mateti, Piezoelectric MEMS sensors: State-of-the-art and perspectives, *Meas. Sci. Technol.* **20**, 092001 (2009).

[3]N. Setter, D. Damjanovic, L. Eng, G. Fox, S. Gevorgian, S. Hong, A. Kingon, H. Kohlstedt, N. Y. Park, G. B. Stephenson, I. Stolitchnov, A. K. Taganstev, D. V. Taylor, T. Yamada and S. Streiffer, Ferroelectric thin films: Review of materials, properties, and applications, *J. Appl. Phys.* **100**, 051606 (2006).

[4]Q. Yu, J. F. Li and W. Sun, Composition–phase structure relationship and thickness-dependent ferroelectricity of rhombohedral phase in [111]-textured Nb-doped Pb(Zr,Ti)O_3 thin films, *Appl. Surf. Sci.* **265**, 334 (2013).

[5]Z. X. Zhu and J. F. Li, A comparative study of fibre-textured and epitaxial Nb-doped $Pb(Zr_{0.53}Ti_{0.47})O_3$ thin films on different substrates, *Appl. Surf. Sci.* **256**, 3880 (2010).

[6]L. Egerton and D. M. Dillon, Piezoelectric and dielectric properties of ceramics with the system potassium sodium niobate, *J. Am. Ceram. Soc.* **42**, 438 (2006).

[7]J. G. Wu, D. Q. Xiao and J. G. Zhu, Potassium-sodium niobate lead-free piezoelectric materials: Past, present, and future of phase boundaries, *Chem. Rev.* **115**, 2559 (2015).

[8]T. Zheng, J. G. Wu, D. Q. Xiao and J. G. Zhu, Recent development in lead-free perovskite piezoelectric bulk materials, *Prog. Mater. Sci.* **98**, 552 (2018).

[9]H. J. Seog, A. Ullah, C. W. Ahn, I. W. Kim, S. Y. Lee and J. Park, Recent progress in potassium sodium niobate lead-free thin films, *J. Korean. Phys. Soc.* **72**, 1467 (2018).

[10]B. Y. Kim, T. G. Seong, I. T. Seo, J. S. Kim, C. Y. Kang, S. J. Yoon and S. Nahm, Effects of oxygen pressure on electrical properties of $(Na_{0.5}K_{0.5})NbO_3$ films grown on Pt/Ti/SiO_2/Si substrates, *Acta Mater.* **60**, 7034 (2012).

[11]T. Li, G. S. Wang, D. Remiens and X. L. Dong, Characteristics of highly (001) oriented (K,Na)NbO_3 films grown on $LaNiO_3$ bottom electrodes by RF magnetron sputtering, *Ceram. Int.* **39**, 1359 (2013).

[12]L. Q. Xu, F. Chen, F. Jin, D. Lan, L. L. Qu, K. X. Zhang, G. Y. Gao and W. B. Wu, Tuning electrical properties and phase transitions through strain engineering in lead-free ferroelectric $K_{0.5}Na_{0.5}NbO_3$-$LiTaO_3$-$CaZrO_3$ thin films, *Appl. Phys. Lett.* **115**, 202901 (2019).

[13]S. Sharma, A. Kumar, V. Gupta and M. Tomar, Dielectric and ferroelectric studies of KNN thin film grown by pulsed laser deposition technique, *Vacuum* **160**, 233 (2019).

[14]X. Y. Yang, Z. J. Cheng, J. Y. Cheng, D. W. Wang, F. Shi, G. P. Zheng and M. S. Cao, Structural and ferroelectric properties of textured KNN thick films prepared by sol-gel methods, *Integr. Ferroelectr.* **176**, 171 (2016).

[15]Y. Nakashima, W. Sakamoto and T. Yogo, Processing of highly oriented (K,Na)NbO_3 thin films using a tailored metal-alkoxide precursor solution, *J. Eur. Ceram. Soc.* **31**, 2497 (2011).

[16]L. L. Yao and K. J. Zhu, Citrate complexing sol-gel process of lead-free (K,Na)NbO_3 ferroelectric films, *Mod. Phys. Lett. B* **30**, 1650157 (2016).

[17]D. Q. Zhang, F. Y. Zheng, X. Y. Yang, L. Z. Feng, X. M. Huang, H. M. Liu and M. S. Cao, Preparation and ferroelectric properties of $K_{0.5}Na_{0.5}NbO_3$ thin films derived from non-alcohol niobium salt sol-gel process, *Integr. Ferroelectr.* **154**, 97 (2014).
[18]Y. Saito, H, Takao, T. Tani, T. Nonoyama, K. Takatori and T. Homma, Lead-free piezoceramics, *Nature* **432**, 84 (2004).
[19]A. F. Solarte, N. Pellegr, O. D. Sanctis and M. G. Stachiotti, Effect of Li- and Ta-doping on the ferroelectric properties of $Na_{0.5}K_{0.5}NbO_3$ thin films prepared by a chelate route, *J. Sol-Gel. Sci. Technol.* **66**, 488 (2013).
[20]E. Hollenstein, D. Damjanovic and N. Setter, Temperature stability of the piezoelectric properties of Li-modified KNN ceramics, *J. Eur. Ceram. Soc.* **27**, 4093 (2007).
[21]D. Li, H. L. Du, F. Tang, F. Luo, D. M. Zhu and W. C. Zhou, Effect of heating rate on the structure evolution of $(K_{0.5}Na_{0.5})$-NbO_3–$LiNbO_3$ lead-free piezoelectric ceramics, *J. Electroceram.* **20**, 107 (2008).
[22]P. Zhao, B. P. Zhang and J. F. Li, High piezoelectric d_{33} coefficient in Li-modified lead-free $(Na,K)NbO_3$ ceramics sintered at optimal temperature, *Appl. Phys. Lett.* **90**, 242909 (2007).
[23]H. L. Du, F. S. Tang, D. J. Liu, D. M. Zhu, W. C. Zhou and S. B. Qu, The microstructure and ferroelectric properties of $(K_{0.5}Na_{0.5})$-NbO_3–$LiNbO_3$ lead-free piezoelectric ceramics, *Mat. Sci. Eng. B-Adv.* **136**, 165 (2007).
[24]C. C. Lin, C. C. Chen, C. M. Weng, S. Y. Chu, C. S. Hong and C. C. Tsai, Effects of lithium doping on microstructure, electrical properties, and chemical bonds of sol-gel derived NKN thin films, *J. Appl. Phys.* **117**, 085307 (2015).
[25]P. C. Goh, K. Yao and Z. Chen, Lithium diffusion in (Li, K, Na)NbO_3 piezoeletric thin films and the resulting approach for enhanced performance properties, *Appl. Phys. Lett.* **99**, 092902 (2011).
[26]Z. X. Zhu, J. F. Li, Y. Y. Liu and J. Y. Li, Shifting of the morphotropic phase boundary and superior piezoelectric response in Nb-doped $Pb(Zr,Ti)O_3$ epitaxial thin films, *Acta Mater.* **57**, 4288 (2009).
[27]Q. Yu, J. F. Li, W. S, Z. Zhou, Y. Xu and Z. K. Xie, Electrical properties of $K_{0.5}Na_{0.5}NbO_3$ thin films grown on Nb:$SrTiO_3$ single-crystalline substrates with different crystallographic orientations, *J. Appl. Phys.* **113**, 024101 (2013).
[28]H. R. Liu, Z. L. Liu and K. L. Yao, Improved electric properties in $BiFeO_3$ films by the doping of Ti, *J. Sol-Gel. Sci. Technol*. **41**, 123 (2007).
[29]J. Pérez de la Cruz, E. Joanni, P. M. Viarinho and A. L. Kholkin, Thickness effect on the dielectric, ferroelectric, and piezoelectric properties of ferroelectric lead zirconate titanate thin films, *J. Appl. Phys.* **108**, 114106 (2010).
[30]M. Cheng, G. Q. Tan, X. Xue, A. Xia and H. J. Ren, Preparation of Nd-doped $BiFeO_3$ films and their electrical properties, *Phys. B* **407**, 3360 (2012).
[31]Y. J. Ren, X. H. Zhu, C. Y. Zhang, J. L. Zhu, J. G. Zhu and D. Q. Xiao, High stable dielectric permittivity and low dielectric loss in sol-gel derived $BiFeO_3$ thin films, *Ceram. Int*. **40**, 2489 (2014).
[32]A. F. Tian, W. Ren, L. Y. Wang, P. Shi, X. F. Chen, X. Q. Wu and X. Yao, Effect of deposition temperature on orientation and electrical properties of $(K_{0.5}Na_{0.5})NbO_3$ thin films by pulsed laser deposition, *Appl. Surf. Sci.* **258**, 2674 (2012).
[33]F. Fu, B, Shen, J. W. Zhai, Z. K. Xu and X. Yao, Electrical properties of Li doped sodium potassium niobate thick films prepared by a tape casting process, *J. Alloys Compd.* **509**, 7130 (2011).
[34]J. G. Wu, J. Wang, D. Q. Xiao and J. G. Zhu, Leakage mechanism of cation-modified $BiFeO_3$ thin film, *AIP Adv.* **1**, 022138 (2011).
[35]C. H. Yang, Y. J. Han, X. S. Sun, J. Chen, J. Qian and L. X. Chen, Effects of Nd^{3+}-substitution for Bi-site on the leakage current, ferroelectric and dielectric properties of $Na_{0.5}Bi_{0.5}TiO_3$ thin films, *Ceram. Int*. **44**, 6330 (2018).
[36]M. Peddigari, B. Sindam, K. C. J. Raju and P. Dobbidi, Optical and microwave dielectric properties of phase pure $(K_{0.5}Na_{0.5})NbO_3$ thin films deposited by RF magnetron sputtering, *J. Am. Ceram. Soc.* **98**, 1444 (2015).
[37]M. Matsubara, T. Yamaguchi, K. Kikuta and S. Hirano, Effect of Li substitution on the piezoelectric properties of potassium sodium niobate ceramics, *Jpn. J. Appl. Phys.* **44**, 6136 (2005).
[38]H. Yang, M, Jain, N. A. Suvorova, H. Zhou, H. M. Luo and D. M. Feldmann, Temperature-dependent leakage mechanisms of $Pt/BiFeO_3/SrRuO_3$ thin film capacitors, *Appl. Phys. Lett.* **91**, 072911 (2007).
[39]Y. H. Zhen and J. F. Li, Abnormal grain growth and new core–shell structure in $(K,Na)NbO_3$-based lead-free piezoelectric ceramics, *J. Am. Ceram. Soc.* **90**, 3496 (2007).
[40]K. Wang and J. F. Li, Domain Engineering of lead-free li-modified $(K,Na)NbO_3$ polycrystals with highly enhanced piezoelectricity, *Adv. Funct. Mater.* **20**, 1924 (2010).
[41]J. Y. Li, J. F. Li, Q, Yu, Q. N. Chen and S. H. Xie, Strain-based scanning probe microscopies for functional materials, biological structures, and electrochemical systems, *J. Materiomics* **1**, 3 (2015).
[42]K. Zhu, B. J. Song, G. L. Ge, J. F. Li, F. Yan and L. X. Xu, Construction of multi-domain coexistence enhanced piezoelectric properties of $Bi_{0.5}Na_{0.5}TiO_3$-based thin films, *J. Eur. Ceram. Soc.* **41**, 6456 (2021).
[43]K. X. Li, F. Wang, M. Deng, K. Hu, D. Y. Song and Y. W. Hao, Microstructure and bending piezoelectric characteristics of AlN film for high-frequency flexible SAW devices, *J. Mater. Sci. Mater. Electron*. **32**, 13146 (2021).
[44]Y. Nakashima, W. Sakamoto, H. Maiwa, T. Shimura and T. Yogo, Lead-free piezoelectric $(K,Na)NbO_3$ thin films derived from metal alkoxide precursors, *Jpn. J. Appl. Phys.* **46**, 311 (2007).
[45]S. S. Won, J. Lee, V. Venugopal and D. Kim, Lead-free Mn-doped $(K_{0.5},Na_{0.5})NbO_3$ piezoelectric thin films for MEMS-based vibrational energy harvester applications, *Appl. Phys. Lett.* **108**, 1131 (2016).
[46]J. S. Kim, C. W. Ahn and A. Ullah, Ferroelectric and electrical properties of lead-free $(K_{0.44}Na_{0.52}Li_{0.04})(Nb_{0.86}Ta_{0.10}Sb_{0.04})O_3$ thin films, *J. Korean. Phys. Soc.* **68**, 1461 (2016).
[47]F. Ni, K. Zhu, L. X. Xu, Y. Liu, H. Yan, B. Shen and J. W. Zhai, Piezoelectric enhancement and vacancy defect reduction of lead-free $Bi_{0.5}Na_{0.5}TiO_3$-based thin films, *Ceram. Int*. **48**, 12601 (2022).
[48]Z. P. Yang, Y. T. Hou, B. Liu and L. L. Wei, Structure and electrical properties of Nd_2O_3-doped $0.82Bi_{0.5}Na_{0.5}TiO_3$-$0.18Bi_{0.5}K_{0.5}TiO_3$ ceramics, *Ceram. Int.* **35**, 1423 (2009).
[49]S. Y. Lee, C. W. Ahn, J. S. Kim, A. Ullah, H. J. Lee and H. Hwang, Enhanced piezoelectric properties of Ta substituted-$(K_{0.5}Na_{0.5})$ NbO_3 films: A candidate for lead-free piezoelectric thin films, *J. Alloys Compd.* **509**, L194 (2011).
[50]M. Abazari, T. Choi, S. W. Cheong and A. Safari, Nanoscale characterization and local piezoelectric properties of lead-free KNN-LT-LS thin films, *J. Phys. D. Appl. Phys.* **43**, 025405 (2010).
[51]L. Wang, R. Z. Zuo, L. D. Liu, H. L. Su, M. Shi and X. C. Chu, Preparation and characterization of sol–gel derived (Li,Ta,Sb) modified $(K,Na)NbO_3$ lead-free ferroelectric thin films, *Mater. Chem. Phys.* **130**, 165 (2011).